processes

MDPI

Article

A Low-Molecular-Weight Polymer Fluid-Loss Additive for Water-Based Drilling Fluids Under High-Salinity, High-Temperature, and High-Density Conditions

Juan Miao [1], Bing Huang [2] and Ge Wang [1,*]

[1] School of Petroleum and Natural Gas Engineering, Southwest Petroleum University, Chengdu 610500, China
[2] China National Petroleum Corporation Chuanqing Drilling Engineering Co., Ltd., Iraq Branch, Chengdu 610051, China
* Correspondence: gw@swpu.edu.cn

Abstract

Maintaining effective fluid-loss control in water-based drilling fluids under coupled high-salinity, high-temperature, and high-density conditions remains a critical challenge in deep and ultra-deep drilling operations. In this study, a low-molecular-weight polymer fluid-loss additive (LM-ASQF) was synthesized via redox-initiated copolymerization of acrylamide, dimethyldiallylammonium chloride, and sodium allyl sulfonate. The synthesis route and proposed polymer structure were further illustrated to clarify the incorporation of amide, quaternary ammonium, and sulfonate functional units within the LM-ASQF molecular architecture. The polymer exhibited a controllable number-average molecular weight of 18.2–29.4 kDa with a unimodal distribution. Thermal analysis confirmed that no main-chain-dominated degradation occurred below 220 °C, indicating structural stability under high-temperature conditions. In drilling-fluid systems containing NaCl, $CaCl_2$, and mixed salts (0–20%), LM-ASQF maintained stable rheological properties, with apparent viscosity ranging from 26.1 to 41.6 mPa·s, while the API fluid loss was controlled within 5.8–11.2 mL. After thermal aging at 220 °C for 16 h, the API fluid loss remained below 13 mL in both freshwater and mixed-salt systems. In high-density systems (1.80–2.40 g/cm^3), the drilling fluids preserved continuous rheological structures and showed no abrupt increase in filtration. Mechanistically, fluid-loss control was primarily attributed to synergistic interfacial adsorption of amide groups, hydration stabilization induced by sulfonate functionalities, and particle rearrangement-driven filter-cake densification, rather than viscosity enhancement through long-chain entanglement. This mechanism enables effective filtration control without excessive viscosity increase, thereby maintaining rheological compatibility under complex conditions. These results demonstrate that the low-molecular-weight design strategy provides a reliable approach for achieving stable fluid-loss control in water-based drilling fluids under high salinity, elevated temperature, and high-density conditions.

Keywords: water-based drilling fluids; low-molecular-weight polymer; fluid-loss control; process adaptability; high-salinity conditions; filter-cake densification

Check for updates

Academic Editor: Paolo Trucillo

Received: 15 April 2026
Revised: 22 June 2026
Accepted: 1 July 2026
Published: 5 July 2026

Copyright: © 2026 by the authors. Licensee MDPI, Basel, Switzerland. This article is an open access article distributed under the terms and conditions of the Creative Commons Attribution (CC BY) license.

1. Introduction

With the continuous exploitation of deep and ultra-deep hydrocarbon resources, maintaining the stability of water-based drilling fluids under coupled high-temperature, high-salinity, and high-density conditions has become increasingly challenging [1,2]. In highly mineralized formations, dissolved ions compress the electrical double layer of clay

and weighting particles, inducing polymer chain contraction, particle aggregation, and deterioration of colloidal stability. These changes typically result in the formation of loose and permeable filter cakes, thereby aggravating filtrate invasion and fluid-loss failure [3–5]. Meanwhile, elevated temperatures accelerate the thermal degradation of conventional polymer additives and weaken their interfacial adsorption capacity, making it difficult to simultaneously maintain rheological continuity and effective filtration control under complex drilling conditions [6–8]. Therefore, developing fluid-loss additives capable of sustaining stable interfacial structures and filtration performance under coupled salinity–temperature–density conditions has become a critical issue in drilling-fluid design. Although several commercial polymers, such as cellulose derivatives, starch-based additives, xanthan gum, and polyacrylamide-based products, have been widely used for fluid-loss control in water-based drilling fluids, their performance is often constrained under deep and ultra-deep drilling conditions. High-molecular-weight commercial polymers generally contribute to viscosity enhancement and filter-cake formation through chain extension and intermolecular entanglement; however, elevated salinity, divalent ions, high temperature, and high solid loading can induce chain contraction, adsorption weakening, aggregation, or thermal degradation. These effects may result in unstable rheology, poor compatibility with high-density formulations, and reduced fluid-loss control efficiency. Therefore, the specific challenge addressed in this work is not the absence of commercial fluid-loss additives, but the lack of a process-compatible polymer that can maintain filtration control without excessive viscosity buildup under simultaneously high-salinity, high-temperature, and high-density conditions.

Recent studies on fluid-loss control materials have gradually converged toward several representative design strategies, including hydration enhancement via functional groups, strengthening of interfacial adsorption, and promotion of filter-cake densification. Liu et al. [9] developed zwitterionic fluid-loss additives and demonstrated that zwitterionic structures can maintain relatively stable hydration and dispersion states in saline media, thereby improving filtration control reliability. Similar zwitterionic and polyzwitterionic filtrate reducers have also been reported to enhance salt resistance through anti-polyelectrolyte behavior, hydration-shell retention, and charge-regulated adsorption under high-salinity conditions [10,11]. However, under more complex conditions involving calcium contamination, mixed salts, and high solid content, maintaining a balance between rheological compatibility and colloidal stability remains challenging. Li et al. [10] proposed nanosilica-reinforced polymer gel systems, where the synergistic effect of nanoparticle filling and polymer adsorption contributes to the formation of compact filter cakes after high-temperature and high-salinity aging. Nevertheless, such systems are highly dependent on nanoparticle dispersion quality and formulation complexity, which may reduce reproducibility and operational robustness, particularly in high-density drilling-fluid systems. Ma et al. [11] further introduced polymer/graphene-oxide composite fluid-loss additives and confirmed that composite architectures can enhance filter-cake structure and suppress filtrate invasion under harsh conditions. Despite these advantages, issues related to cost, dispersion controllability, and field adaptability still limit the broader application of nanoparticle-containing systems. In addition to synthetic polymer and nanocomposite systems, environmentally oriented and process-compatible additives have recently received increasing attention, reflecting the need to balance filtration control, rheological compatibility, and environmental acceptability [7].

In contrast, low-molecular-weight polymer systems have emerged as a promising alternative strategy. Liu et al. [12] demonstrated that effective fluid-loss reduction can be achieved without significant viscosity enhancement, thereby improving rheological compatibility. However, the quantitative relationships among molecular structure, interfacial

behavior, and filter-cake evolution in low-molecular-weight systems—especially under multivalent ion environments and coupled high-temperature and high-density conditions—remain insufficiently understood. Earlier studies on multicomponent copolymer systems also provide useful insights. Bai and Yang [13] reported an AM/AMPS/DMDAAC/SSS quaternary copolymer and demonstrated that the synergistic incorporation of anionic, cationic, and sulfonate functionalities can improve fluid-loss control in saline drilling fluids, although such systems still involve trade-offs among formulation complexity, molecular-weight controllability, and economic feasibility.

Overall, current strategies can be broadly categorized into two main routes. One relies on structuralized or composite architectures to enhance filter-cake densification, but this approach often increases formulation complexity and reduces engineering robustness [7,14,15]. The other emphasizes reducing molecular weight to avoid excessive viscosity buildup; however, it still lacks systematic understanding of how low-molecular-weight polymers regulate interfacial structure and filtration behavior under coupled high-salinity, especially divalent-ion-rich, and high-temperature conditions [16–19]. Recent studies have further extended this strategy by developing low-molecular-weight filtrate reducers, laponite–polymer composites, polymer nanocomposites, and network-structured polymers with reduced viscosity effects for high-temperature water-based drilling fluids [20–23]. As a result, there remains a clear need to clarify the structure–interface–filter-cake relationship in low-molecular-weight systems and to establish design principles for achieving effective fluid-loss control while maintaining rheological compatibility.

Under this context, low-molecular-weight polymer fluid-loss additives provide a promising pathway for addressing these challenges. Compared with conventional commercial polymers that mainly rely on long-chain entanglement or bulk viscosity enhancement, LM-ASQF was designed to regulate filtration behavior through a different mechanism, namely low-molecular-weight chain diffusion, multipoint interfacial adsorption, hydration stabilization, and particle-scale filter-cake reconstruction. The incorporation of amide, sulfonate, and quaternary ammonium groups into one copolymer chain was intended to combine hydrogen-bond adsorption, salt-tolerant hydration, and electrostatic interaction, thereby improving compatibility with high-salinity and high-density drilling-fluid systems. This molecular design enables the construction of stable hydration layers and multipoint interfacial adsorption structures, while controlled molecular-weight distribution facilitates dispersion stability and particle-scale filter-cake reconstruction under saline and high-temperature conditions. In this study, a low-molecular-weight polymer fluid-loss additive was designed and systematically investigated. Its molecular structure, molecular-weight characteristics, thermal stability, and solution conformation behavior were characterized, and its rheological properties, fluid-loss control performance, shale inhibition, lubrication behavior, and biotoxicity were evaluated in drilling-fluid systems under varying salinity, temperature, and density conditions. Particular emphasis was placed on elucidating the dominant mechanisms governing fluid-loss control, including interfacial adsorption, hydration stabilization, and filter-cake densification. The objective is to establish a clear structure–performance–mechanism relationship and to provide guidance for the design of fluid-loss additives suitable for complex drilling environments.

2. Experimental Section

2.1. Materials and Instruments

(1) Materials: Acrylamide (AM, ≥99%) was supplied by Aladdin Reagent Co., Ltd. (Shanghai, China). Dimethyldiallylammonium chloride (DMDAAC, 65% aqueous solution) was purchased from Xiya Reagent Co., Ltd. (Zaozhuang, China). Sodium allyl sulfonate (SAS, ≥98%) was obtained from J&K Scientific Ltd. (Beijing, China). Ammonium persulfate

(APS, ≥98%) was provided by Aladdin Reagent Co., Ltd. (Shanghai, China), and sodium bisulfite ($NaHSO_3$, ≥98%) was purchased from Tianjin Guangfu Fine Chemical Co., Ltd. (Tianjin, China). Sodium hydroxide, anhydrous ethanol, and inorganic salts (NaCl and $CaCl_2$) were of analytical grade and purchased from Sinopharm Chemical Reagent Co., Ltd. (Shanghai, China). API-grade sodium bentonite was purchased from Qingdao Haitongda Special Instrument Co., Ltd. (Qingdao, China) and used as the clay phase for preparing the base drilling fluid, and sodium carbonate (Na_2CO_3, analytical grade) was used as a bentonite hydration regulator. API-grade barite powder was purchased from Qingdao Haitongda Special Instrument Co., Ltd. (Qingdao, China) and used as the weighting material for preparing high-density drilling-fluid systems. The barite had a $BaSO_4$ content of 92.6%, an apparent density of 4.25 g/cm^3, and a particle-size distribution of D10 = 3.8 μm, D50 = 16.5 μm, and D90 = 45.2 μm. Deionized water (resistivity ≥18.2 MΩ·cm) was used throughout all experiments.

Shale samples used for inhibition tests were obtained from drilling-site cores in a shale gas block in the Sichuan Basin, China, dried, crushed, and sieved to obtain uniform particle sizes prior to use.

(2) Instruments: Fourier transform infrared (FTIR) spectra were recorded using a Nicolet iS50 spectrometer (Thermo Fisher Scientific, Waltham, MA, USA). Elemental composition was analyzed using a Vario EL Cube elemental analyzer (Elementar Analysensysteme GmbH, Langenselbold, Germany). Molecular-weight characteristics were determined by gel permeation chromatography (PL-GPC 220, Agilent Technologies, Santa Clara, CA, USA). Thermal behavior was examined using a simultaneous thermogravimetric–differential scanning calorimeter (STA 449 F5, Netzsch, Selb, Germany). Dynamic light scattering (DLS) and zeta potential measurements were conducted using a Zetasizer Nano ZS (Malvern Panalytical, Malvern, UK). Rheological properties were measured using a ZNN-D6 rotational viscometer (Qingdao Tongchun Petroleum Instrument Co., Ltd., Qingdao, China). High-temperature aging tests were performed using a high-pressure aging cell (Qingdao Haitongda Special Instrument Co., Ltd., Qingdao, China). API fluid loss was evaluated using a standard API filtration apparatus (Qingdao Tongchun Petroleum Instrument Co., Ltd., Qingdao, China). Shale linear swelling was measured using a linear swelling tester, and rolling recovery tests were conducted using a rolling recovery apparatus (Qingdao Haitongda Special Instrument Co., Ltd., Qingdao, China). Lubrication performance was evaluated using an extreme-pressure lubricity tester (Qingdao Tongchun Petroleum Instrument Co., Ltd., Qingdao, China). Biotoxicity was assessed using a luminescent bacteria toxicity analyzer (Ecolight Biotechnology Co., Ltd., Beijing, China). Data processing, statistical analysis, and figure plotting were performed using Microsoft Excel 2021 (Microsoft Corporation, Redmond, WA, USA) and OriginPro 2024 (OriginLab Corporation, Northampton, MA, USA).

2.2. Preparation of the Fluid-Loss Additive

Under a nitrogen atmosphere, acrylamide (AM), dimethyldiallylammonium chloride (DMDAAC), and sodium allyl sulfonate (SAS) were sequentially dissolved in deionized water at a mass ratio of 6:3:1. The total monomer mass fraction was adjusted to 25%. The solution was magnetically stirred at 300 rpm for 30 min until a homogeneous mixture was obtained. The pH of the solution was adjusted to 7.0–7.5 using a dilute sodium hydroxide solution. The reaction mixture was heated to 55 °C in a thermostatic water bath under continuous stirring. Subsequently, a redox initiator system consisting of ammonium persulfate (APS) and sodium bisulfite ($NaHSO_3$) was added. To investigate the effect of initiator dosage on molecular-weight regulation, the total initiator content, defined as the combined mass fraction of APS and $NaHSO_3$ relative to the total monomer mass, was varied

from 0.20% to 0.40%. The mass ratio of APS to $NaHSO_3$ was kept constant at 4:3 throughout the synthesis. Unless otherwise specified, the LM-ASQF sample prepared at a total initiator content of 0.30% was used for subsequent structural characterization and drilling-fluid performance evaluation. The mass fractions of APS and $NaHSO_3$ relative to the total monomer content were 0.20% and 0.15%, respectively. The copolymerization reaction was allowed to proceed for 3 h under constant stirring at 300 rpm. After completion of the reaction, the system was cooled to room temperature. The obtained polymer solution was then transferred to an oven and maintained at 90 °C for 16 h. The solution was subsequently poured into anhydrous ethanol at a volume ratio of 1:5 (polymer solution:ethanol) to induce precipitation. The precipitated product was collected by centrifugation at 4000 rpm for 10 min and washed twice with ethanol. Finally, the product was dried under vacuum at 60 °C to constant weight, yielding a light-colored powder, denoted as LM-ASQF.

The schematic synthesis route and proposed molecular structure of LM-ASQF are shown in Figure 1. Under the APS/$NaHSO_3$ redox initiation system, acrylamide, dimethyldiallylammonium chloride, and sodium allyl sulfonate were copolymerized through a free-radical polymerization pathway, resulting in a low-molecular-weight random copolymer containing amide, quaternary ammonium, and sulfonate functional units. The amide groups provide potential hydrogen-bonding and interfacial adsorption sites, the sulfonate groups contribute to hydration stabilization and salt tolerance, and the quaternary ammonium groups participate in electrostatic interaction and dispersion stabilization. Therefore, the proposed molecular structure provides the structural basis for the subsequent fluid-loss control and filter-cake densification behavior.

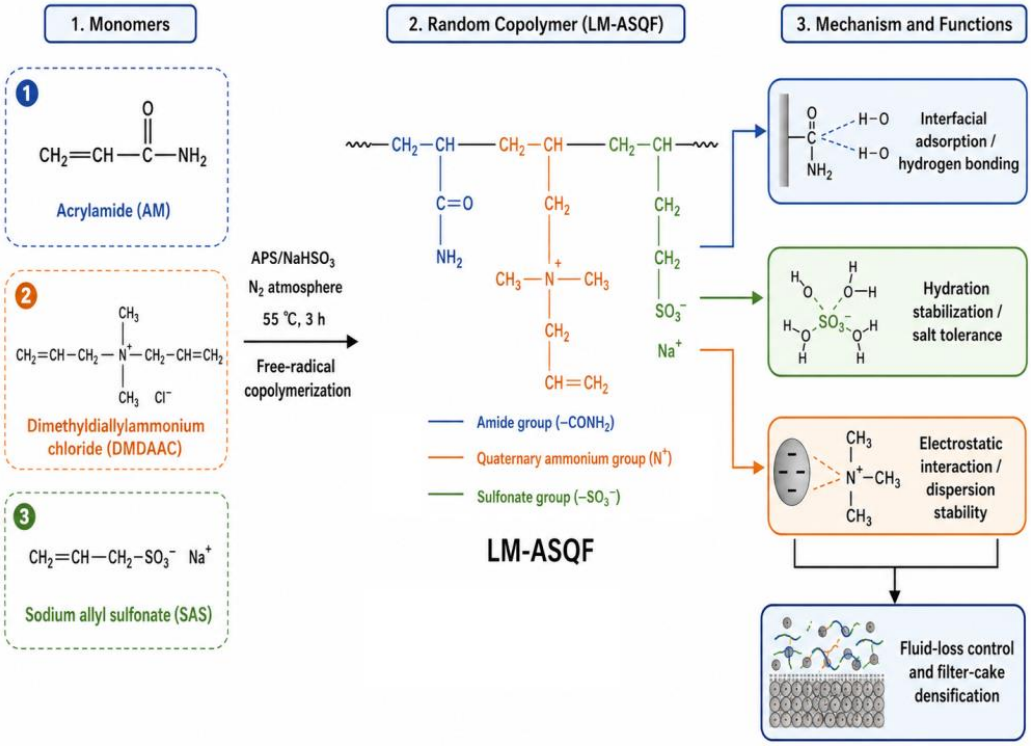


Figure 1. Schematic synthesis route, proposed molecular structure, and functional group–regulated fluid-loss control mechanism of LM-ASQF.

2.3. Experimental Methods

2.3.1. Molecular Structure and Elemental Composition Characterization

The molecular structure of LM-ASQF was characterized using Fourier transform infrared spectroscopy (FTIR) and elemental analysis. FTIR measurements were performed on freeze-dried polymer samples using a spectrometer in the wavenumber range of

4000–400 cm^{-1}, with a resolution of 4 cm^{-1} and 32 scans per sample. Elemental analysis was conducted to determine the mass fractions of carbon (C), hydrogen (H), nitrogen (N), and sulfur (S) in the polymer samples. To further verify the chemical structure of LM-ASQF, proton nuclear magnetic resonance (^{1}H NMR) spectroscopy was performed. The purified and vacuum-dried LM-ASQF sample was dissolved in D_2O, and the spectrum was recorded at room temperature using the residual solvent signal as the chemical-shift reference. The ^{1}H NMR spectrum was used to identify the characteristic proton signals of the polymer backbone and AM-, DMDAAC-, and SAS-derived structural units, and to verify the conversion of vinyl monomers during copolymerization.

2.3.2. Molecular Weight and Distribution Analysis

The molecular weight and molecular-weight distribution of LM-ASQF were determined by gel permeation chromatography (GPC). Prior to analysis, the polymer samples were dissolved in deionized water and filtered through a 0.45 μm membrane to remove insoluble impurities. The measurements were performed using an aqueous GPC system with deionized water as the mobile phase at a flow rate of 1.0 $mL \cdot min^{-1}$. The column temperature was maintained at 30 °C. A refractive index detector was used for signal acquisition. Calibration was carried out using polyethylene glycol (PEG) standards with known molecular weights. The number-average molecular weight (Mn), weight-average molecular weight (Mw), and polydispersity index (PDI = Mw/Mn) were calculated based on the calibration curve.

2.3.3. Thermal Stability Analysis

Thermal stability was evaluated using simultaneous thermogravimetric–differential scanning calorimetry (TG–DSC). The measurements were carried out under a nitrogen (N_2) atmosphere with a gas flow rate of 50 mL/min. The samples (approximately 5–10 mg) were placed in alumina crucibles and heated from 30 to 800 °C at a heating rate of 10 °C/min. Mass-loss behavior was recorded from the TG curves, and the corresponding heat-flow signals were obtained from the DSC curves.

2.3.4. Dissolution Behavior and Conformational Characteristics in Aqueous Solution

The dissolution behavior and conformational characteristics of LM-ASQF in aqueous solution were characterized using dynamic light scattering (DLS) and zeta potential measurements. Polymer solutions with a mass fraction of 1.0% were prepared in deionized water and stirred at 25 °C. At different dissolution times, the hydrodynamic diameter (Dh), polydispersity index (PDI), and zeta potential were measured. DLS measurements were performed at a fixed scattering angle of 173°, and each sample was equilibrated for 2 min prior to measurement. Zeta potential measurements were conducted under the same temperature conditions. Solution viscosity was measured using a rotational viscometer at 25 °C. All measurements were carried out in electrolyte-free systems.

2.3.5. Drilling Fluid Formulation and Rheological Measurements

Water-based drilling fluids were prepared using a unified base formulation. The base drilling fluid was prepared by dispersing 4.0 wt% API-grade sodium bentonite and 0.30 wt% Na_2CO_3 in deionized water. The suspension was stirred at 800 rpm for 30 min and then prehydrated for 24 h at room temperature to obtain a stable bentonite-based base fluid. Unless otherwise specified, no additional commercial fluid-loss reducer, viscosifier, plugging agent, or dispersant was added to the base fluid. LM-ASQF was added at a mass fraction of 1.5%. The required amount of polymer was gradually introduced into the prehydrated base fluid under continuous stirring at 800 rpm and mixed for 30 min to ensure complete dispersion. Saline environments were established by adding NaCl, $CaCl_2$, or

mixed salts at different mass fractions after complete dispersion of LM-ASQF. For the mixed-salt systems, NaCl and $CaCl_2$ were used at a mass ratio of 3:1, and the reported mixed-salt concentration refers to the total mass fraction of NaCl and $CaCl_2$ in the drilling fluid. Accordingly, the 10% mixed-salt system contained 7.5% NaCl and 2.5% $CaCl_2$, whereas the 20% mixed-salt system contained 15.0% NaCl and 5.0% $CaCl_2$. Unless otherwise specified, "mixed salts" in subsequent tests refers to this NaCl/$CaCl_2$ formulation. In this study, "base fluid" refers to the bentonite-based formulation without LM-ASQF, whereas "LM-ASQF-treated drilling fluid" refers to the same base formulation containing 1.5 wt% LM-ASQF. The prepared drilling fluids were aged under sealed conditions at specified temperatures for 16 h prior to testing. Rheological properties, including apparent viscosity (AV), plastic viscosity (PV), and yield stress (YP), were measured using a rotational viscometer at 25 °C according to standard procedures. AV, PV, and YP were calculated based on dial readings at 600 and 300 rpm. All rheological measurements were conducted using three independently prepared drilling-fluid samples, and the results are reported as mean ± standard deviation (n = 3).

2.3.6. Fluid-Loss Performance Evaluation

Fluid-loss performance was evaluated using the standard API filtration test. Measurements were conducted under prescribed pressure and time conditions, and the filtrate volume collected per unit time was recorded as the API fluid loss. All filtration tests were performed after rheological measurements to ensure consistent sample states. Both pre- and post-aging samples were evaluated following identical procedures to assess the impact of high-temperature exposure on fluid-loss control. To further evaluate the filtration-control capability of LM-ASQF under direct high-temperature and high-pressure conditions, HTHP fluid-loss tests were conducted using a high-temperature high-pressure filtration apparatus. The drilling-fluid samples were thermally equilibrated at 180 °C or 220 °C and then tested under a differential pressure of 3.5 MPa for 30 min. The collected filtrate volume was recorded as the HTHP fluid loss. In addition, a representative 2.40 g/cm^3 barite-weighted drilling-fluid system was selected to evaluate the HTHP filtration behavior under coupled high-temperature and high-density conditions. API fluid-loss tests were also performed in triplicate using independently prepared samples, and the results are expressed as mean ± standard deviation (n = 3).

2.3.7. High-Temperature Aging Procedure

To simulate high-temperature drilling conditions, drilling fluid samples were aged in sealed aging cells at 180 °C or 220 °C for 16 h. After aging, samples were allowed to cool naturally to room temperature prior to subsequent rheological, fluid-loss, inhibition, and lubrication performance evaluations.

2.3.8. Shale Inhibition Performance Tests

Shale inhibition performance was assessed using linear swelling and rolling recovery tests. The linear swelling test quantified shale expansion height (He) in drilling fluids, while the rolling recovery test was used to calculate shale recovery rate (Rr). Measurements were conducted under different saline environments and before and after high-temperature aging to evaluate the ability of the drilling fluids to suppress shale hydration and swelling.

2.3.9. Lubrication Performance Evaluation

Lubrication performance was evaluated by measuring the friction coefficient (f) of drilling fluids, from which the drag-reduction rate (Dr) was calculated. Tests were performed at room temperature and after high-temperature aging to analyze the effects of temperature and salinity on lubrication behavior.

2.3.10. High-Density Drilling Fluid Systems and Performance Testing

High-density water-based drilling fluid systems with densities ranging from 1.80 g/cm^3 to 2.40 g/cm^3 were prepared by introducing API-grade barite powder as the weighting agent under a unified formulation framework. The barite powder had an apparent density of 4.25 g/cm^3 and a particle-size distribution of D10 = 3.8 μm, D50 = 16.5 μm, and D90 = 45.2 μm. The target densities were adjusted by gradually adding barite under continuous stirring, and the same barite source and particle-size grade were used for all high-density formulations to minimize variability caused by weighting-material properties. Rheological properties, fluid-loss performance, shale inhibition, and lubrication behavior were evaluated before and after thermal aging to assess the overall adaptability of LM-ASQF under high-density and high-temperature conditions.

2.3.11. Compatibility Evaluation with Representative Drilling Fluid Formulations

To evaluate the applicability of LM-ASQF under more realistic drilling-fluid conditions, compatibility tests were conducted using representative water-based drilling-fluid formulations. LM-ASQF was incorporated into different formulations containing typical components, including bentonite, inorganic salts, weighting agents, shale inhibitors, and lubricating additives. The tested formulations included a freshwater bentonite-based system, a NaCl-containing saline system, a $CaCl_2$-containing divalent-ion system, a high-density barite-weighted system, and a multi-additive field-oriented formulation. All formulations were prepared under the same mixing procedure and aged at 220 °C for 16 h. Rheological parameters, API fluid loss, apparent sedimentation behavior, and visible flocculation were recorded to assess the compatibility of LM-ASQF with different drilling-fluid components.

2.3.12. Filter-Cake Morphology and Thickness Characterization

To directly examine the filter-cake structure formed by LM-ASQF, filter-cake morphology and thickness were characterized using a representative mixed-salt drilling-fluid system after thermal aging. The base drilling fluid without LM-ASQF and the LM-ASQF-treated drilling fluid were aged at 220 °C for 16 h and then subjected to API filtration under identical conditions. The obtained filter cakes were carefully removed, dried at 60 °C to constant weight, and cut into small sections for morphological observation. The surface and cross-sectional morphologies were observed by scanning electron microscopy (SEM). In addition, the filter-cake thickness was measured at five different positions for each sample, and the average value was calculated from three independently prepared filter cakes.

2.3.13. Biotoxicity Evaluation

Biotoxicity of the drilling fluid systems was evaluated using an acute luminescent bacteria toxicity assay. Prior to testing, drilling fluid samples were subjected to solid–liquid separation, and the liquid phase was collected for analysis. Luminescence inhibition (I) was measured, and the median effective concentration (EC50) was calculated to assess the influence of LM-ASQF dosage and high-temperature aging on drilling fluid biotoxicity. The biotoxicity test was used as an indicator of the acute ecological compatibility of the fluid system under the tested conditions, rather than as a comprehensive evaluation of environmental friendliness or biodegradability.

3. Results and Discussion

3.1. Structural Characteristics and Physicochemical Basis of LM-ASQF

3.1.1. Molecular Structure and Functional Group Distribution

The proposed synthesis route and molecular structure of LM-ASQF are illustrated in Figure 1. To further verify the chemical structure of the synthesized polymer, the molecular

structural characteristics of LM-ASQF were elucidated through combined analysis of ^{1}H NMR, FTIR, and elemental composition results, as shown in Figures 2–4.

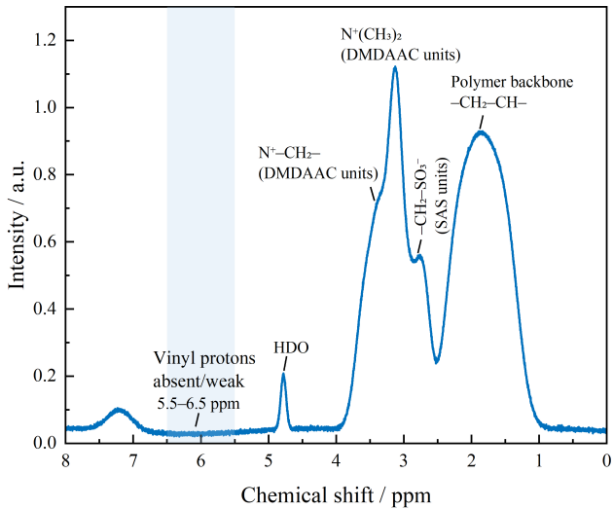


Figure 2. ^{1}H NMR spectrum of LM-ASQF in D_2O.

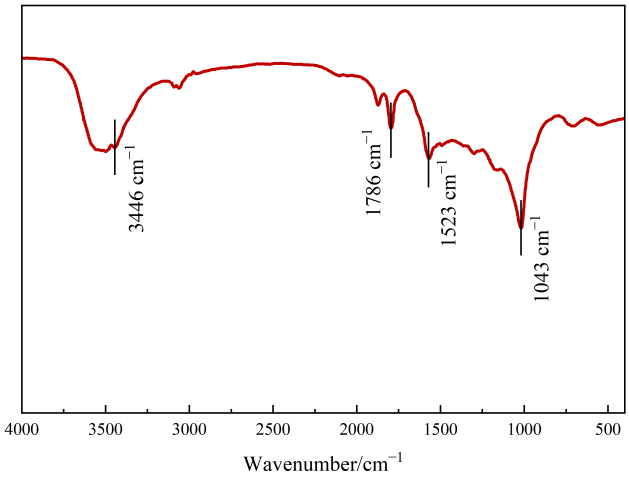


Figure 3. Fourier transform infrared (FTIR) spectrum of LM-ASQF.

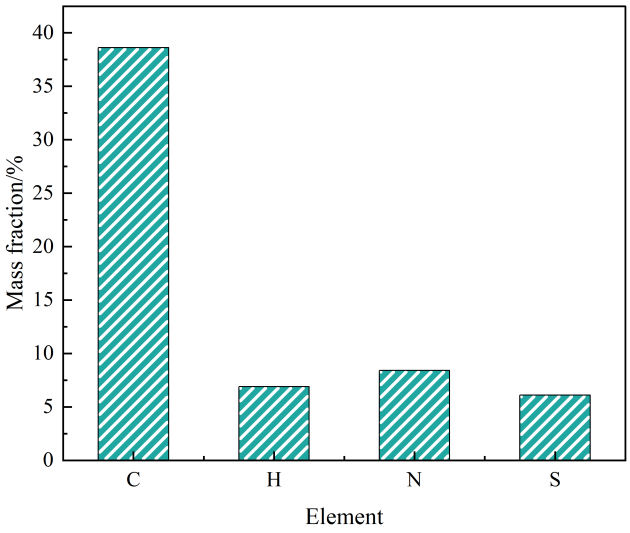


Figure 4. Elemental composition of LM-ASQF.

The ^{1}H NMR spectrum of LM-ASQF is shown in Figure 2. Broad resonance signals in the range of 1.2–2.4 ppm are assigned to the saturated methylene and methine protons of the copolymer backbone, indicating the formation of polymer chains after free-radical copolymerization. The signals at approximately 2.7–3.0 ppm are attributed to methylene protons adjacent to sulfonate groups derived from SAS, while the signals around 3.1–3.6 ppm correspond to methyl and methylene protons adjacent to quaternary ammonium groups derived from DMDAAC. In addition, the absence or substantial weakening of vinyl proton signals in the range of 5.5–6.5 ppm supports the successful conversion of vinyl monomers into the copolymer structure. These NMR results confirm the formation of a saturated polymer backbone and provide direct evidence for the incorporation of SAS-derived sulfonate units and DMDAAC-derived quaternary ammonium units into LM-ASQF. Considering the broad and partially overlapped proton signals of water-soluble random copolymers, the ^{1}H NMR spectrum was used mainly to verify the incorporation of characteristic monomer units rather than to determine an exact sequence-level bonding ratio.

As shown in Figure 3, a broad and intense absorption band centered at 3446 cm^{-1} is observed, which is primarily attributed to the N–H stretching vibration of amide groups. This band partially overlaps with hydrogen-bond vibrations involving polymer chain segments and residual bound water, indicating the presence of strong hydrogen-bonding interactions within the polymer system. In the mid-wavenumber region, a characteristic absorption peak appears at 1523 cm^{-1}, corresponding to the amide II band arising from the coupled N–H bending and C–N stretching vibrations, providing further evidence for the successful incorporation of amide structural units along the polymer backbone. In the low-wavenumber region, a strong and sharp absorption peak at 1043 cm^{-1} is assigned to the symmetric stretching vibration of S=O bonds in sulfonate groups, confirming the stable presence of sulfonate functionalities within the polymer structure. A weak absorption signal is detected at 1786 cm^{-1}; however, its low intensity and deviation from the typical amide carbonyl signature suggest that it is more likely associated with local variations in the carbonyl chemical environment or hydrogen-bond-induced vibrational shifts rather than a dominant structural motif of the polymer.

Elemental analysis results (Figure 4) show that the mass fractions of C, H, N, and S in LM-ASQF are 38.6%, 6.9%, 8.4%, and 6.1%, respectively. The sulfur content is consistent with the feed ratio of the sulfonate monomer, while nitrogen originates from both amide and quaternary ammonium functionalities. These results collectively confirm the synergistic incorporation of amphoteric functional groups within a single polymer chain. The coexistence of electrically neutral backbone segments, anionic sites, and cationic sites endows the polymer with a multi-charged architecture, providing a structural basis for multipoint adsorption and interfacial interaction under high-salinity conditions.

Overall, the molecular architecture of LM-ASQF features the concurrent introduction of amide and sulfonate hydrophilic functional groups, whose cooperative distribution establishes a robust structural foundation for polymer solubility, interfacial activity, and salt tolerance in water-based drilling fluid systems. Among them, the amide groups provide hydrogen-bonding and interfacial adsorption sites, the sulfonate groups contribute to hydration stabilization and salt tolerance, and the quaternary ammonium groups participate in electrostatic interaction with negatively charged clay or weighting-particle surfaces. More importantly, the simultaneous presence of sulfonate anionic groups and quaternary ammonium cationic groups gives LM-ASQF a zwitterionic molecular architecture at the polymer-chain level. This zwitterionic feature does not refer to a single monomeric zwitterion, but to the coexistence of oppositely charged functional units within the same copolymer chain, which provides a molecular basis for electrostatic regulation, hydration stabilization, multipoint adsorption, and salt-tolerant dispersion stability.

3.1.2. Molecular-Weight Distribution and Controlled Low-Molecular-Weight Characteristics

To evaluate the molecular-weight response under different initiator conditions, LM-ASQF samples were synthesized using total initiator contents of 0.20–0.40%, where the total initiator content refers to the combined mass fraction of APS and $NaHSO_3$ relative to the total monomer mass. The statistical results are summarized in Table 1, and the corresponding GPC traces are shown in Figure 5.

Table 1. Effect of total initiator content, defined as the combined mass fraction of APS and $NaHSO_3$ relative to the total monomer mass, on the molecular-weight characteristics of LM-ASQF.

Total Initiator Content/%	Mn/kDa	Mw/kDa	PDI
0.20	29.4	62.1	2.11
0.25	26.3	57.4	2.18
0.30	23.1	51.2	2.22
0.35	20.5	46.8	2.28
0.40	18.2	42.1	2.31

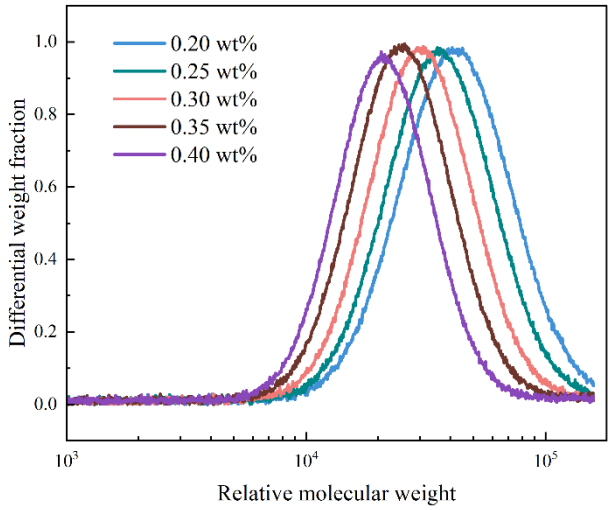


Figure 5. GPC molecular-weight distribution curves of LM-ASQF synthesized with different total initiator contents.

As shown in Table 1, the number-average molecular weight (Mn) of LM-ASQF is concentrated within the range of 18.2–29.4 kDa, while the weight-average molecular weight (Mw) spans 42.1–62.1 kDa. This overall molecular-weight level is substantially lower than that of conventional high-molecular-weight polyacrylamide-based fluid-loss additives. With increasing total initiator content from 0.20 to 0.40%, both Mn and Mw exhibit a continuous decreasing trend. Specifically, Mn decreases from 29.4 to 18.2 kDa, corresponding to a total reduction of 11.2 kDa, while Mw decreases from 62.1 to 42.1 kDa, corresponding to a total reduction of 20.0 kDa. These results indicate that the increased radical concentration effectively restricts chain propagation during free-radical copolymerization, thereby enabling controllable molecular-weight regulation. Correspondingly, the polydispersity index (PDI) increases modestly from 2.11 to 2.31, suggesting that the molecular-weight distribution remains reasonably broad within the low-molecular-weight regime without developing bimodal features or abnormal tailing.

From the distribution profiles (Figure 5), all samples display unimodal and continuous molecular-weight distributions, and no high-molecular-weight tailing is detected. This behavior is consistent with the absence of crosslinking reactions and the deliberately controlled reaction duration during synthesis. A moderately broadened distribution within

the low-molecular-weight range is advantageous for generating multiscale adsorption units, enabling polymer chains of different lengths to participate in filter-cake construction in a dispersed manner rather than relying on long-chain entanglement for fluid-loss reduction.

Further analysis of the correlation between initiator dosage and molecular-weight evolution shows that the decreases in Mn and Mw become relatively moderate within the initiator range of 0.30–0.35%. This suggests that the chain-growth and chain-termination processes tend to reach a more stable regulation state within this dosage window. This molecular-weight window effectively avoids chain-coil collapse and bridging flocculation commonly observed for high-molecular-weight polymers in high-salinity environments, while still providing an appropriate molecular size for forming compact adsorption layers on clay particle surfaces.

Overall, LM-ASQF exhibits a stable and well-controlled molecular-weight distribution concentrated in the low-to-medium molecular-weight range, which can be precisely regulated through initiator dosage. This low-molecular-weight characteristic provides direct structural support for maintaining good dispersion stability and reliable fluid-loss control in high-salinity and high-temperature water-based drilling fluid systems.

3.1.3. Thermal Stability and High-Temperature Structural Retention

The thermogravimetric behavior and associated thermal effects of LM-ASQF are shown in Figure 6, where the mass-loss process exhibits a clearly staged profile. In the revised Figure 4, the DSC curve is presented together with the TG curve to correlate the staged mass-loss behavior with the corresponding heat-flow response.

As indicated by the TG–DSC curves in Figure 6, the thermal degradation of LM-ASQF can be divided into three successive stages. The first stage occurs within the temperature range of 30–150 °C and is associated with a mass loss of 3.2%, which is mainly attributed to the removal of physically adsorbed water and a small fraction of weakly bound water. The corresponding DSC curve shows only a weak endothermic response in this region, indicating that this stage is dominated by water desorption rather than backbone-related thermal transition or decomposition. The second stage appears between 150 and 320 °C, during which the cumulative mass loss increases to 12.7%. In this region, the DSC curve exhibits a broad and relatively weak endothermic feature, which can be associated with thermal relaxation and partial cleavage of side-chain functionalities, particularly quaternary ammonium and sulfonate groups, while the main-chain framework remains continuous. The third stage is concentrated in the range of 320–520 °C, where the mass-loss rate increases markedly, as evidenced by a steeper TG slope accompanied by a pronounced endothermic response in the DSC curve. This temperature interval corresponds to substantive thermal decomposition of the polymer backbone and can be regarded as the primary degradation stage of LM-ASQF.

Notably, at 220 °C, the cumulative mass loss of LM-ASQF is limited to only 6.4%, and the TG curve remains smooth without abrupt changes, indicating that the polymer does not undergo main-chain-dominated thermal decomposition below this temperature. The DSC signal around 220 °C also remains within a weak heat-flow response region, further supporting that the polymer mainly experiences localized side-chain relaxation rather than severe backbone degradation at this temperature. From the perspective of residual mass, a char yield of 41.3% is retained at 800 °C, suggesting that nitrogen- and sulfur-containing functional groups contribute to suppressing thermal decomposition and enhancing structural retention at elevated temperatures.

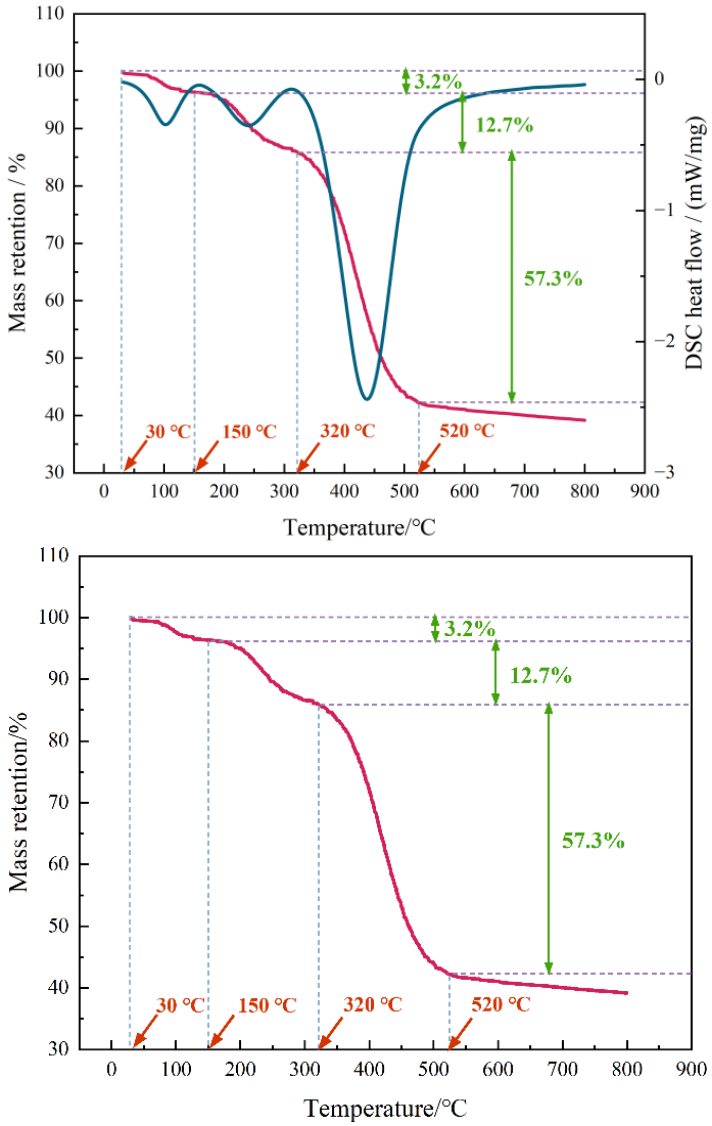


Figure 6. TG–DSC curves of LM-ASQF under a nitrogen atmosphere, showing the relationship between staged mass loss and the corresponding heat-flow response. The pink curve represents the TG mass-retention curve, and the blue curve represents the DSC heat-flow curve. The green arrows indicate the staged mass-loss percentages, the orange arrows indicate characteristic temperatures, and the light-blue dashed vertical lines mark the boundaries of the main thermal stages.

Taken together, the TG–DSC results confirm that LM-ASQF retains its basic structural integrity after thermal exposure below 220 °C, and its thermal mass loss in this temperature regime is dominated primarily by side-chain adjustment and localized structural relaxation. The combined TG–DSC evidence further demonstrates that the major thermal decomposition process occurs mainly within 320–520 °C, which is substantially higher than the thermal-aging temperature used in the drilling-fluid performance evaluation. These results provide thermal analysis support for the subsequent evaluation of drilling-fluid performance after high-temperature aging, rather than direct evidence of in situ service performance at 220 °C.

3.1.4. Solution Conformation Evolution and Dispersion Stability

LM-ASQF aqueous solutions exhibit pronounced evolution in particle size and interfacial charge characteristics as a function of dissolution time. The corresponding trends are summarized in Figure 7.

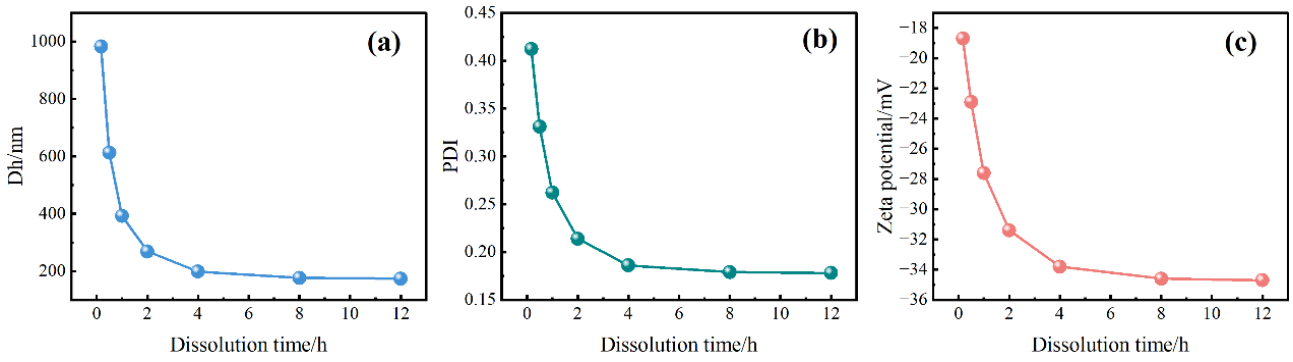


Figure 7. Evolution of particle size distribution and interfacial charge characteristics of LM-ASQF aqueous solutions at different dissolution times. (**a**) Variation of hydrodynamic diameter (Dh) with dissolution time; (**b**) Variation of polydispersity index (PDI) with dissolution time; (**c**) Variation of zeta potential with dissolution time.

As can be seen from Figure 7, the dissolution process of LM-ASQF is characterized by a continuous transition involving rapid particle-size convergence, progressive narrowing of size distribution, and enhanced electrostatic stabilization. During the early dissolution stage, the hydrodynamic diameter (Dh) decreases sharply from 982.6 nm at 0.17 h to 268.5 nm at 2.00 h, corresponding to a reduction of 714.1 nm. With further extension of dissolution time to 4.00–12.00 h, Dh converges into a narrow range of 198.7–173.9 nm, indicating that the system enters a stable hydrated conformational state at later stages. In parallel with particle-size convergence, the PDI decreases from 0.412 to 0.178, reflecting the progressive disintegration of large aggregates and homogenization of dispersed units, which markedly reduces size heterogeneity within the system. Meanwhile, the absolute value of the zeta potential increases from 18.7 mV to 34.7 mV, demonstrating enhanced electrostatic repulsion and colloidal stability after dissolution is completed. This behavior is consistent with the synergistic incorporation of anionic sulfonate and cationic quaternary ammonium groups within the polymer structure, which promotes hydration-layer formation and interfacial charge redistribution.

These results indicate that the dissolution of LM-ASQF is not merely a macroscopic solubilization process, but rather a microscopic transition from loosely associated, large-scale aggregates to stable, hydrated conformational units. After approximately 4.00 h of dissolution, Dh stabilizes within the range of 173.9–198.7 nm, the PDI decreases to below 0.186, and the zeta potential remains stable at −33.8 to −34.7 mV. The simultaneous appearance of plateau behavior in all three parameters confirms that the solution conformation and dispersion state reach a steady condition beyond this time point. Accordingly, this dissolution duration can be adopted as a unified pre-dissolution condition for subsequent performance evaluations, including rheological, fluid-loss, lubrication, and inhibition tests, thereby minimizing data variability arising from differences in dissolution degree.

3.2. Process Performance Evaluation Under Complex Drilling Conditions

3.2.1. Process Response Under Salinity Variation

Under different saline environments, the rheological behavior and fluid-loss response of LM-ASQF-treated drilling fluids exhibit systematic variations. The corresponding results are summarized in Tables 2 and 3. The standard deviations of the rheological and fluid-loss data are relatively small compared with the salinity-induced changes, indicating that the observed decreasing viscosity trend and increasing fluid-loss trend are reproducible rather than caused by experimental fluctuation.

Table 2. Rheological parameters of drilling fluids under different salinity conditions.

Salt System	Salt Concentration/%	Apparent Viscosity/mPa·s	Plastic Viscosity/mPa·s	Yield Stress/Pa
Salt-free	0	41.6 ± 0.5	24.3 ± 0.4	17.3 ± 0.3
NaCl	5	38.9 ± 0.6	22.6 ± 0.4	16.3 ± 0.3
	10	35.7 ± 0.5	20.8 ± 0.3	14.9 ± 0.3
	15	33.2 ± 0.6	19.3 ± 0.4	13.9 ± 0.2
	20	31.4 ± 0.7	18.1 ± 0.4	13.3 ± 0.3
$CaCl_2$	5	32.8 ± 0.6	19.4 ± 0.4	13.4 ± 0.3
	10	28.7 ± 0.5	16.9 ± 0.3	11.8 ± 0.2
	15	26.1 ± 0.6	15.3 ± 0.3	10.8 ± 0.3
Mixed salts	10	30.5 ± 0.6	18.2 ± 0.4	12.3 ± 0.3
	20	27.6 ± 0.7	16.1 ± 0.4	11.5 ± 0.3

Note: In the mixed-salt systems, NaCl and $CaCl_2$ were mixed at a mass ratio of 3:1, and the listed salt concentration represents the total mass fraction of NaCl and $CaCl_2$.

Table 3. API fluid loss of drilling fluids under different salinity conditions.

Salt System	Salt Concentration/%	API Fluid Loss/mL
Salt-free	0	5.8 ± 0.2
NaCl	5	6.4 ± 0.2
	10	7.2 ± 0.3
	15	7.9 ± 0.3
	20	8.6 ± 0.4
$CaCl_2$	5	7.2 ± 0.3
	10	9.1 ± 0.4
	15	10.9 ± 0.5
Mixed salts	10	9.4 ± 0.4

As shown in Table 2, under salt-free conditions, the drilling fluid exhibits an apparent viscosity of 41.6 mPa·s, a plastic viscosity of 24.3 mPa·s, and a yield stress of 17.3 Pa, indicating favorable cuttings-carrying capacity and flow stability. With increasing NaCl concentration from 5 to 20%, the apparent viscosity gradually decreases from 38.9 to 31.4 mPa·s, while the plastic viscosity declines from 22.6 to 18.1 mPa·s. These reductions remain within a controlled range, and no abrupt viscosity collapse or flocculation behavior is observed. The corresponding yield stress is consistently maintained between 13.3 and 15.1 Pa, suggesting that the shear-bearing structure of the drilling fluid is not severely disrupted by monovalent salt enrichment.

In $CaCl_2$-containing systems, the rheological parameters show higher sensitivity to salt concentration, reflecting the stronger charge-screening effect of divalent cations. At a $CaCl_2$ concentration of 10%, the apparent viscosity and plastic viscosity remain at 28.7 and 16.9 mPa·s, respectively, indicating preservation of a continuous rheological framework. When the concentration is further increased to 15%, the apparent viscosity decreases to 26.1 mPa·s; however, no abrupt structural breakdown is observed, demonstrating that LM-ASQF retains a certain buffering capacity against divalent-ion-induced destabilization. In mixed-salt systems, the evolution of rheological parameters falls between those observed in NaCl- and $CaCl_2$-dominated systems, showing a gradual but controlled decline with increasing salinity.

Based on the maintained rheological stability, the API fluid-loss control performance of LM-ASQF under different salinity conditions was further evaluated, as presented in Table 3. In the salt-free system, the API fluid loss is limited to 5.8 mL, demonstrating effective filtration control. With increasing NaCl concentration up to 20%, the API fluid loss increases moderately to 8.6 mL, corresponding to an increment of only 2.8 mL, which remains well below the uncontrolled filtration levels typically observed in conventional water-based drilling fluids under high-salinity conditions. In $CaCl_2$ systems, the API fluid loss increases from 7.2 to 10.9 mL as the salt concentration rises, yet the increase follows a continuous and predictable trend without runaway behavior. For mixed-salt systems, API fluid loss is stabilized within the range of 9.4–11.2 mL, indicating that LM-ASQF maintains functional adaptability under complex electrolyte environments.

Overall, LM-ASQF exhibits a synergistic response characterized by "gradual rheological attenuation coupled with controllable fluid loss" under high-salinity conditions. The structural weakening induced by increasing salt concentration is confined within an acceptable range, and the corresponding increase in fluid loss proceeds in a slow, quasi-linear manner rather than exhibiting abrupt destabilization. This performance profile provides a stable rheological and filtration foundation for subsequent application in high-temperature and high-density drilling fluid systems.

In summary, across NaCl-, $CaCl_2$-, and mixed-salt environments, LM-ASQF effectively suppresses fluid-loss escalation while preserving the essential rheological framework of drilling fluids, demonstrating strong salt tolerance and reliable fluid-loss control capability.

3.2.2. Salt Resistance and Filtration Stability

The variations in rheological behavior and fluid-loss performance of LM-ASQF-treated drilling fluids before and after high-temperature aging are summarized in Tables 4 and 5.

Table 4. Changes in rheological parameters of drilling fluids before and after high-temperature aging.

System	Aging Temperature/°C	Apparent Viscosity/mPa·s	Plastic Viscosity/mPa·s	Yield Stress/Pa	Viscosity Retention/%
Freshwater	Unaged	41.6	24.3	17.3	100.0
	180	36.9	21.8	15.1	88.7
	220	33.8	19.6	14.2	81.3
Mixed salts	Unaged	30.5	18.2	12.3	100.0
	180	25.9	15.6	10.8	85.0
	220	23.8	14.2	9.6	78.0

Table 5. API and HTHP fluid loss of LM-ASQF-treated drilling fluids under high-temperature conditions.

System	Density/(g/cm^3)	Aging/Test Temperature/°C	API Fluid Loss After Cooling/mL	HTHP Fluid Loss/mL
Freshwater	—	Unaged	5.8	—
	—	180	7.1	13.8
	—	220	8.3	19.6
Mixed salts	—	Unaged	9.4	—
	—	180	11.2	17.6
	—	220	12.6	24.8
High-density barite-weighted system	2.40	220	12.1	25.6

As shown in Table 4, in the freshwater system, the apparent viscosity decreases from 41.6 to 36.9 mPa·s after aging at 180 °C, corresponding to a viscosity retention of 88.7%. When the aging temperature is increased to 220 °C, the apparent viscosity further decreases to 33.8 mPa·s, with a retention of 81.3%. Plastic viscosity and yield stress exhibit similar downward trends with increasing temperature; however, all changes occur gradually without abrupt degradation, indicating preservation of the continuous shear-bearing structure.

In mixed-salt systems, high-temperature aging exerts a slightly stronger impact on rheological properties. After aging at 180 °C, the apparent viscosity decreases from 30.5 to 25.9 mPa·s (retention of 85.0%), and further decreases to 23.8 mPa·s at 220 °C (retention of 78.0%). Despite this measurable attenuation, the drilling fluids maintain an intact rheological framework, with no evidence of flocculation or structural collapse. This indicates that LM-ASQF does not rely on excessive viscosity buildup to achieve fluid-loss control, but instead maintains a moderate shear-bearing structure under thermal and saline stress.

Building upon the retained rheological structure, the influence of high-temperature aging on fluid-loss control was further examined, as presented in Table 5.

In the freshwater system, the API fluid loss increases from 5.8 mL under unaged conditions to 7.1 mL after aging at 180 °C, and to 8.3 mL at 220 °C, corresponding to an overall increment of 2.5 mL. In the mixed-salt system, the API fluid loss rises from 9.4 mL to 12.6 mL after aging at 220 °C. In both cases, the increase follows a continuous and predictable trend, without exhibiting runaway filtration behavior.

Notably, even after aging at 220 °C, the API fluid loss of both freshwater and mixed-salt systems remains below 13 mL, demonstrating that LM-ASQF retains effective fluid-loss suppression capability following high-temperature exposure. This indicates that the fluid-loss control function does not undergo structural failure upon thermal aging. However, because API fluid loss measured after cooling cannot fully represent filtration behavior under actual high-temperature and pressure-driven conditions, HTHP fluid-loss tests were further conducted at 180 °C and 220 °C.

As shown in Table 5, the HTHP fluid loss of the freshwater system is 13.8 mL at 180 °C and 19.6 mL at 220 °C, while that of the mixed-salt system is 17.6 mL and 24.8 mL, respectively. These values are higher than the corresponding API fluid loss measured after cooling, which is reasonable because elevated temperature and pressure enhance filtrate invasion. Nevertheless, the HTHP fluid loss remains within a controlled range, and no abrupt filtration failure is observed. For the representative 2.40 g/cm^3 high-density barite-weighted system, the HTHP fluid loss at 220 °C is 25.6 mL, indicating that LM-ASQF still maintains filtration-control capability under coupled high-temperature and high-density conditions. This behavior can be attributed to the combined effects of interfacial adsorption, hydration stabilization, and particle-scale filter-cake densification.

Overall, under high-temperature aging up to 220 °C, LM-ASQF-treated water-based drilling fluids maintain a continuous rheological structure and controllable fluid-loss performance. High-temperature exposure induces a quantifiable but moderate attenuation in viscosity level and filtration control; however, the degradation process is gradual, predictable, and does not compromise the fundamental structural integrity or functional effectiveness of the drilling fluid system. The supplemented HTHP results further confirm that LM-ASQF maintains controllable filtration behavior under direct high-temperature and high-pressure conditions. This performance retention provides a robust stability foundation for the application of LM-ASQF in high-temperature and high-density water-based drilling fluid systems.

3.2.3. Inhibition and Lubrication Compatibility Under Salinity and Thermal Aging

The effects of LM-ASQF on shale stability and drilling-fluid friction behavior under different salinity conditions and high-temperature aging are summarized in Tables 6 and 7.

Table 6. Shale inhibition performance of drilling fluids under different salinity and aging conditions.

System	Salt Concentration/%	Aging Temperature/°C	He/mm	Rr/%
Salt-free	0	Unaged	1.26	84.3
	0	220	1.58	78.6
NaCl	10	Unaged	1.12	86.9
	10	220	1.44	80.2
Mixed salts	10	Unaged	1.38	82.1
	10	220	1.67	76.5

Table 7. Lubrication performance parameters of drilling fluids under different salinity and aging conditions.

System	Salt Concentration (%)	Aging Temperature (°C)	f	Dr (%)
Salt-free	0	Unaged	0.192	38.6
		220	0.214	31.4
NaCl	10	Unaged	0.187	40.2
		220	0.209	33.7
Mixed salts		Unaged	0.205	33.1
		220	0.228	28.7

As shown in Table 6, under salt-free conditions, the unaged system exhibits a linear swelling height (He) of 1.26 mm with a corresponding rolling recovery rate (Rr) of 84.3%. After aging at 220 °C, He increases to 1.58 mm, and Rr decreases to 78.6%; however, the overall inhibition performance remains within an acceptable range. Under NaCl conditions (10%), the unaged system shows a He of 1.12 mm and an Rr of 86.9%, indicating that the saline environment does not cause severe deterioration in shale inhibition behavior. After aging at 220 °C, He increases to 1.44 mm, and Rr decreases to 80.2%, following a trend consistent with that of the salt-free system. In mixed-salt environments, He ranges from 1.38 to 1.67 mm, and Rr remains within 76.5–82.1%, suggesting that the LM-ASQF-containing system maintains acceptable inhibition compatibility even under complex electrolyte conditions.

The lubrication behavior of the drilling-fluid systems is summarized in Table 7. In the salt-free system, the friction coefficient (f) increases from 0.192 under unaged conditions to 0.214 after aging at 220 °C, accompanied by a reduction in drag-reduction rate (Dr) from 38.6% to 31.4%. Although some attenuation is observed after thermal aging, the lubrication behavior remains controllable. Under NaCl conditions (10%), f increases from 0.187 to 0.209 after high-temperature aging, with a variation trend similar to that of the salt-free system. In mixed-salt systems, f ranges from 0.205 to 0.228, and Dr remains within 28.7–33.1%, indicating that no severe deterioration in lubrication compatibility occurs under combined high-salinity and high-temperature-aging conditions.

Taken together, the inhibition and lubrication results indicate that LM-ASQF primarily functions as a fluid-loss additive without causing pronounced impairment to these auxiliary properties. With increasing salinity and thermal aging, both inhibition and lubrication performance show moderate and predictable changes, while remaining within a serviceable range under the tested conditions. This behavior suggests that LM-ASQF possesses good compatibility with the multi-property requirements of water-based drilling-fluid systems, rather than serving as a dedicated inhibition or lubrication enhancer.

3.2.4. Process Adaptability in High-Density Water-Based Drilling Fluid Systems

The multi-property responses of drilling fluids at different densities are summarized in Tables 8 and 9.

Table 8. Rheological and fluid-loss parameters of drilling fluids at different densities.

Density/(g/cm^3)	Aging Condition	Apparent Viscosity/mPa·s	Plastic Viscosity/mPa·s	Yield Stress/Pa	API Fluid Loss/mL
1.80	Unaged	39.2	23.1	15.6	6.4
2.00		42.8	25.6	16.8	7.6
2.20		45.1	27.3	17.9	8.7
2.40		47.6	29.4	18.9	9.8
1.80	220 °C	33.6	20.2	14.1	8.9
2.00		35.9	21.8	14.9	9.7
2.20		37.4	23.1	15.6	10.8
2.40		38.7	24.6	16.2	12.1

Table 9. Inhibition and lubrication performance parameters of drilling fluids at different densities.

Density/(g/cm^3)	Aging Condition	He/mm	Rr/%	f	Dr/%
1.80	Unaged	1.34	83.6	0.198	36.2
2.00		1.42	81.5	0.205	34.1
2.20		1.53	80.1	0.214	31.8
2.40		1.61	78.9	0.221	29.7
1.80	220 °C	1.52	78.1	0.214	33.7
2.00		1.63	76.4	0.221	31.4
2.20		1.74	75.2	0.229	28.9
2.40		1.86	73.8	0.236	26.4

As shown in Table 8, under unaged conditions, increasing the fluid density from 1.80 to 2.40 g/cm^3 leads to a gradual rise in apparent viscosity (from 39.2 to 47.6 mPa·s) and plastic viscosity (from 23.1 to 29.4 mPa·s), while the yield stress remains within a relatively narrow range of 15.6–18.9 Pa. These trends indicate that the incorporation of weighting agents does not disrupt the shear structure of the drilling fluid. Meanwhile, the API fluid loss increases continuously from 6.4 to 9.8 mL, without exhibiting uncontrolled escalation at higher densities.

After aging at 220 °C, the rheological parameters of the high-density systems decrease overall but retain coherent structural characteristics. At a density of 2.40 g/cm^3, the apparent viscosity, plastic viscosity, and API fluid loss are 38.7 mPa·s, 24.6 mPa·s, and 12.1 mL, respectively, all remaining within acceptable operational limits. These results demonstrate that the LM-ASQF-treated system maintains both rheological integrity and fluid-loss control under combined high-density and high-temperature conditions.

Building on the retention of rheological and fluid-loss performance, the effects of increasing density on shale inhibition and lubrication behavior are further analyzed in Table 9. Under unaged conditions, as density increases from 1.80 to 2.40 g/cm^3, the linear swelling height (He) increases moderately from 1.34 mm to 1.61 mm, while the rolling recovery rate (Rr) decreases from 83.6% to 78.9%, indicating only a limited attenuation of inhibition performance. After aging at 220 °C, He ranges from 1.52 mm to 1.86 mm, and Rr remains within 73.8–78.1%, confirming that effective suppression of shale hydration is preserved even under high-density and high-temperature conditions.

In terms of lubrication behavior, the friction coefficient (f) increases gradually with density from 0.198 to 0.221 under unaged conditions, and from 0.214 to 0.236 after high-temperature aging. Correspondingly, the drag-reduction rate (Dr) remains within 26.4–33.7%, indicating that frictional resistance remains controllable and does not deteriorate markedly with increasing density.

Overall, the multi-property responses under varying density and high-temperature aging conditions demonstrate that LM-ASQF exhibits robust comprehensive adaptability in high-density water-based drilling fluid systems. With increasing density, rheological parameters, fluid loss, inhibition, and lubrication performance all evolve in a predictable and continuous manner, without the occurrence of single-property failure or pronounced performance imbalance. Even after aging at 220 °C, all key indicators remain within engineeringly acceptable ranges, confirming that LM-ASQF can synergistically support the multi-performance requirements of drilling fluids under high-density and high-temperature conditions.

3.2.5. Compatibility with Representative Drilling Fluid Formulations

To further evaluate the practical applicability of LM-ASQF, its compatibility with representative water-based drilling-fluid formulations was examined. The results are summarized in Table 10. Compared with the simplified single-condition tests, these formulations included typical drilling-fluid components such as bentonite, inorganic salts, barite weighting agents, shale inhibitors, and lubricating additives, thereby providing a more realistic basis for assessing formulation compatibility.

Table 10. Compatibility of LM-ASQF with representative water-based drilling-fluid formulations after aging at 220 °C for 16 h.

Formulation	Main Components	Apparent Viscosity/mPa·s	Plastic Viscosity/mPa·s	Yield Stress/Pa	API Fluid Loss/mL	Compatibility Observation
F1	Freshwater bentonite + LM-ASQF	33.8	19.6	14.2	8.3	No visible flocculation
F2	Bentonite + 10% NaCl + LM-ASQF	30.6	18.1	12.5	9.4	Stable dispersion
F3	Bentonite + 5% $CaCl_2$ + LM-ASQF	28.4	16.8	11.6	10.7	Slight viscosity reduction, no phase separation
F4	High-density barite-weighted system + LM-ASQF	38.7	24.6	16.2	12.1	No severe sedimentation
F5	Multi-additive formulation + LM-ASQF	35.2	22.4	14.8	11.4	Good formulation compatibility

The compatibility results show that LM-ASQF maintains stable rheological and filtration-control performance in different water-based drilling-fluid formulations. In

the freshwater bentonite-based system, the apparent viscosity and API fluid loss after aging at 220 °C are 33.8 mPa·s and 8.3 mL, respectively, indicating that LM-ASQF remains effective in a conventional clay-based drilling-fluid environment. In the NaCl-containing system, the API fluid loss remains controlled at 9.4 mL, suggesting that monovalent salt enrichment does not cause severe deterioration in LM-ASQF performance. In the $CaCl_2$-containing system, a moderate reduction in rheological parameters is observed, which is consistent with the stronger charge-screening effect of divalent cations; nevertheless, no visible flocculation or phase separation occurs, and the API fluid loss remains within a controlled range.

For the high-density barite-weighted formulation, LM-ASQF maintains an apparent viscosity of 38.7 mPa·s and an API fluid loss of 12.1 mL after aging, indicating that the polymer is compatible with high-solid and high-density drilling-fluid conditions. Because the same API-grade barite with a fixed particle-size distribution was used throughout the high-density tests, the observed rheological and filtration responses mainly reflect the interaction between LM-ASQF and the barite-weighted drilling-fluid matrix rather than variations in weighting-material properties. In the multi-additive formulation containing typical shale-inhibition and lubrication components, the drilling fluid retains continuous rheological behavior and controlled filtration performance, with no obvious adverse interaction among additives. These results demonstrate that LM-ASQF does not rely on a narrowly defined laboratory formulation, but can maintain functional compatibility across representative water-based drilling-fluid systems.

Overall, the compatibility tests confirm that LM-ASQF can be incorporated into different drilling-fluid formulations without causing severe flocculation, sedimentation, excessive viscosity increase, or filtration-control failure. This compatibility is attributed to its low-molecular-weight structure, zwitterionic charge regulation, and interfacial adsorption-driven filtration mechanism. These characteristics support the practical applicability of LM-ASQF in realistic drilling-fluid environments, particularly under high-temperature, high-salinity, and high-density conditions.

3.2.6. Direct Evidence for Filter-Cake Densification

To further verify the proposed filter-cake densification mechanism, the morphology and thickness of representative filter cakes formed in the mixed-salt system after aging at 220 °C were examined, as shown in Figure 8. As shown in Figure 8a, the surface of the filter cake formed by the base fluid without LM-ASQF is relatively loose, with obvious interparticle voids and an uneven particle arrangement. Figure 8b further shows that the corresponding cross-sectional structure is relatively porous and discontinuous, indicating that the particles are not effectively packed into a compact barrier layer. In contrast, the filter cake formed in the presence of LM-ASQF exhibits a much denser and more continuous surface morphology, as shown in Figure 8c, with markedly fewer visible pores and a tighter particle arrangement. The cross-sectional image in Figure 8d also confirms that the internal structure becomes more compact and continuous after the addition of LM-ASQF, suggesting a reduced number of transport channels for filtrate invasion.

Consistent with the SEM observations, Figure 8e shows that the average filter-cake thickness decreases from 0.82 ± 0.05 mm for the base fluid to 0.54 ± 0.04 mm for the LM-ASQF-treated system. The combined evidence from Figure 8a–e demonstrates that LM-ASQF promotes the formation of a thinner and denser filter cake, rather than merely increasing the bulk viscosity of the drilling fluid. Therefore, the improved fluid-loss control can be reasonably attributed to particle-scale structural reconstruction and filter-cake densification during filtration.

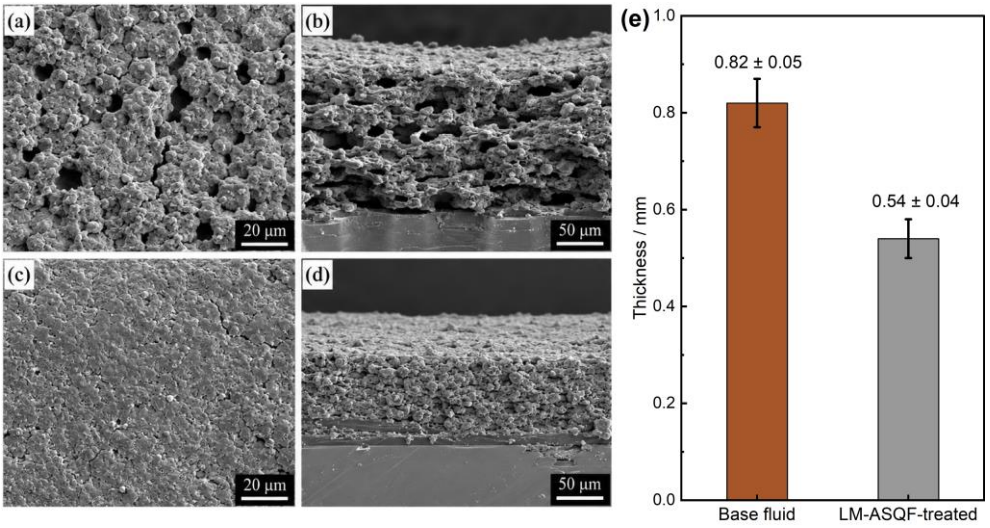


Figure 8. SEM images and thickness comparison of filter cakes formed by the base fluid and LM-ASQF-treated drilling fluid in the mixed-salt system after aging at 220 °C: (**a**) surface morphology of the base-fluid filter cake; (**b**) cross-sectional morphology of the base-fluid filter cake; (**c**) surface morphology of the LM-ASQF-treated filter cake; (**d**) cross-sectional morphology of the LM-ASQF-treated filter cake; (**e**) average filter-cake thickness.

3.2.7. Biotoxicity Response and Environmental Compatibility

The biotoxicity responses of LM-ASQF-treated drilling fluids under different dosages and aging conditions are presented in Figure 9.

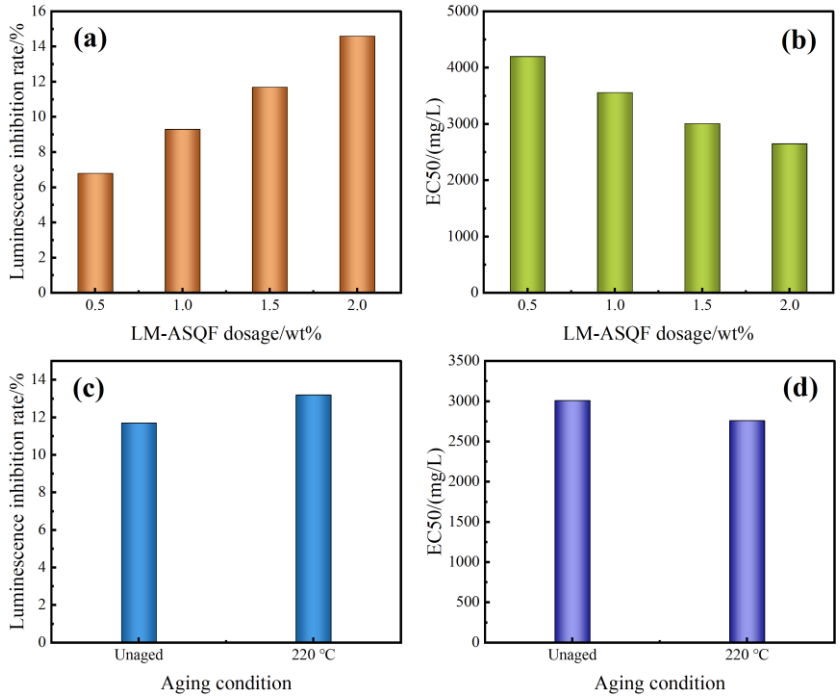


Figure 9. Effects of LM-ASQF on the biotoxicity characteristics of drilling fluid systems. (**a**) Luminescence inhibition rate of drilling fluids at different LM-ASQF dosages; (**b**) EC50 values of drilling fluids at different LM-ASQF dosages; (**c**) Luminescence inhibition rate of drilling fluids before and after high-temperature aging (LM-ASQF 1.5%); (**d**) EC50 values of drilling fluids before and after high-temperature aging (LM-ASQF 1.5%).

As shown in Figure 9a, increasing the LM-ASQF dosage from 0.5% to 2.0% leads to a gradual rise in the luminescence inhibition rate (I) from 6.8% to 14.6%. The overall variation

remains limited, and no abrupt increase in toxicity is observed with increasing dosage. Correspondingly, the EC50 value decreases from 4200 mg/L to 2650 mg/L (Figure 9b), yet remains within the low-toxicity range, indicating that LM-ASQF exerts only a weak inhibitory effect on microbial activity within the typical application dosage window.

Under practical drilling conditions, drilling fluids are commonly subjected to high-temperature circulation; therefore, the influence of thermal aging on biotoxicity was further evaluated after aging at 220 °C for 16 h. As illustrated in Figure 9c, thermal aging results in a slight increase in the luminescence inhibition rate, while the magnitude of change remains well controlled. For example, at an LM-ASQF dosage of 1.5%, the inhibition rate increases from 11.7% before aging to 13.2% after aging. The corresponding EC50 value decreases moderately from 3010 mg/L to 2760 mg/L (Figure 9d). Overall, high-temperature aging does not induce a qualitative shift in toxicity level.

Taken together, the results obtained under different dosages and aging conditions confirm that LM-ASQF-treated water-based drilling fluids exhibit generally weak inhibitory effects on luminescent bacteria, with toxicity variations showing continuous and predictable trends rather than abrupt escalation. Notably, all EC_{50} values remain above 2500 mg/L across the tested conditions, demonstrating favorable acute biotoxicity characteristics and acceptable environmental compatibility under the tested conditions. These results support the low acute toxicity profile of the LM-ASQF-containing drilling-fluid system, but do not by themselves constitute a comprehensive assessment of environmental friendliness or biodegradability.

3.3. Mechanism of Fluid-Loss Control and Filter-Cake Stabilization by Low-Molecular-Weight Polymers

From a molecular-structure perspective, the amide-related absorptions and the characteristic sulfonate S=O bands observed in the FTIR spectra confirm that LM-ASQF incorporates a multipolar functional-group architecture. Such structural motifs simultaneously provide hydrogen-bond donor/acceptor sites and strongly hydrated anionic centers in the aqueous phase. Consistent with this structural evidence, solution-state analyses show that, with increasing dissolution time, the LM-ASQF aqueous system exhibits a continuous decrease in hydrodynamic diameter (Dh), a reduction in polydispersity index (PDI), and an increase in the absolute value of the zeta potential, indicating a transition from an initially aggregated state toward a more stable and well-dispersed configuration. This evolution is consistent with an interfacial adsorption pathway in which low-molecular-weight polymer chains progressively wet and cover particle surfaces, form a stable hydration layer, and thereby reduce effective interparticle attraction. Specifically, amide groups can establish hydrogen-bond interactions with hydroxyl groups and edge-site active centers on clay surfaces, while sulfonate groups enhance interfacial repulsion through strong hydration and charge contributions, collectively suppressing salt-induced aggregation. The zwitterionic molecular architecture of LM-ASQF further strengthens this interfacial regulation mechanism. In high-salinity environments, the sulfonate groups provide strongly hydrated anionic sites that resist dehydration and ion-induced collapse, whereas the quaternary ammonium groups introduce cationic centers capable of interacting with negatively charged clay and weighting-particle surfaces. The coexistence of these oppositely charged units within one low-molecular-weight copolymer chain enables localized charge compensation and multipoint adsorption, thereby reducing salt-induced polymer contraction and particle aggregation. This zwitterionic regulation helps maintain a stable dispersion state under NaCl, $CaCl_2$, and mixed-salt conditions, which is consistent with the controlled rheological attenuation and limited increase in API fluid loss observed in the salinity-resistance tests.

In contrast to conventional fluid-loss control mechanisms dominated by chain entanglement of high-molecular-weight polymers, LM-ASQF is more likely to function through

the combined effects of adsorption-layer thickness and hydration-layer strength. In NaCl and mixed-salt systems, monovalent ions primarily compress the electrical double layer and reduce the repulsive distance between particles; however, the strongly hydrated sulfonate sites of LM-ASQF are still able to maintain an effective hydration shell on particle surfaces, allowing dispersion states to evolve continuously rather than collapse abruptly. In $CaCl_2$ systems, the stronger double-layer compression and bridging effects associated with divalent cations lead to a more pronounced increase in fluid loss, which is consistent with the well-established dependence of interfacial repulsive barriers on electrolyte valence.

At the level of filtration control, the role of LM-ASQF can be described as "filter-cake densification driven by particle-scale structural reconstruction." The low-molecular-weight nature of the polymer implies a higher diffusion coefficient, enabling more efficient migration toward the filtration interface and active participation in filter-cake formation under high-solid conditions. Once adsorbed onto clay and weighting-material surfaces, LM-ASQF can reduce the characteristic size of particle aggregates and improve the continuity of the particle-size distribution. Simultaneously, under filtration pressure, the modified interparticle interactions facilitate the filling and rearrangement of fine particles within pore channels, thereby decreasing filter-cake permeability and suppressing filtrate invasion. This mechanism rationalizes the experimental observation that effective fluid-loss control is achieved without relying on substantial viscosity enhancement: while macroscopic rheological parameters change only moderately, the API fluid loss remains well controlled, indicating that the dominant control factor lies in filter-cake structure and pore connectivity rather than bulk viscosity.

Regarding thermal stability, TG analysis demonstrates that LM-ASQF possesses a relatively high onset temperature for thermal decomposition, supporting the conclusion that the material can retain its interfacial adsorption and structural regulation capability after aging at 220 °C. Consequently, the preservation of performance under high-temperature conditions is more plausibly attributed to the persistence of functional-group hydration and interfacial adsorption, rather than to the formation of new chemical bonds or irreversible structural transformations.

Overall, by integrating structural characterization and solution-state behavior, LM-ASQF is shown to achieve fluid-loss control under high-salinity and high-temperature conditions through a synergistic pathway involving amide-mediated hydrogen-bond adsorption, sulfonate-driven strong hydration stabilization, and dispersion-induced filter-cake densification. A schematic illustration of this structure–interface–filtration performance mechanism is provided in Figure 10.

From a practical perspective, the molecular design of LM-ASQF also considers cost, scalability, and commercial applicability. The monomers used in this study, including acrylamide, dimethyldiallylammonium chloride, and sodium allyl sulfonate, are commercially available water-soluble monomers, and the synthesis is based on conventional aqueous redox-initiated free-radical copolymerization under mild conditions. Compared with nanoparticle-containing, graphene-based, or highly crosslinked composite additives, this route avoids the need for complex dispersion control, expensive nanofillers, or multi-step post-modification. In addition, the low-molecular-weight design allows filtration control to be achieved primarily through interfacial adsorption and filter-cake densification rather than excessive viscosity enhancement, which is beneficial for maintaining pumpability and rheological compatibility in high-density drilling fluids. Although a full techno-economic evaluation and field-scale validation remain necessary before commercialization, the simple monomer system, mild synthesis conditions, and compatibility with conventional water-based drilling-fluid formulations indicate that LM-ASQF has potential for scalable production and practical application in deep and ultra-deep drilling operations.

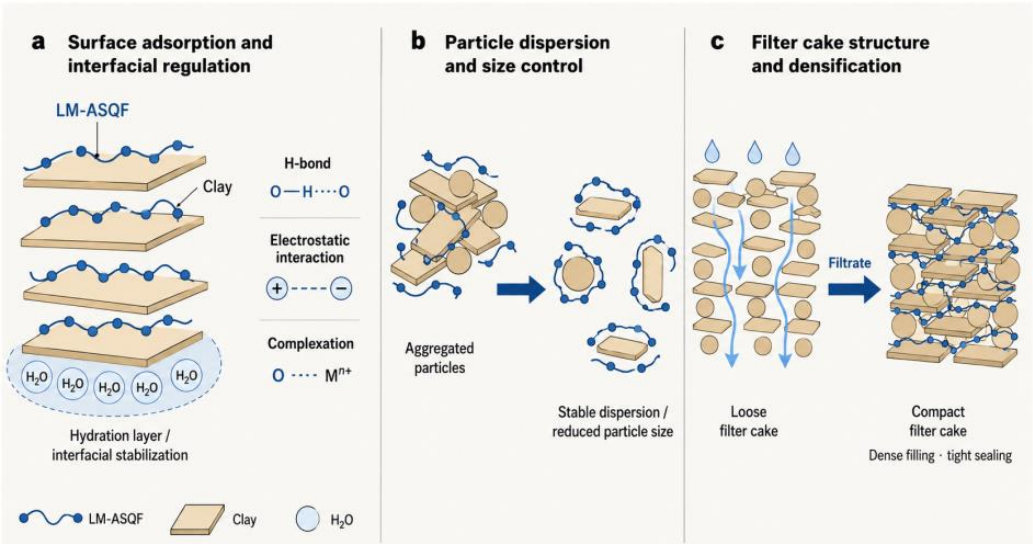


Figure 10. Schematic illustration of the structure–interface–filtration performance mechanism of LM-ASQF in water-based drilling fluids. The blue arrows indicate the filtrate-flow direction through the filter-cake structure.

4. Conclusions

(1) The synthesized LM-ASQF exhibits a well-defined amphiphilic and zwitterionic molecular architecture, where amide, sulfonate, and quaternary ammonium groups are synergistically incorporated into a single polymer backbone. This functional group integration provides a strong structural foundation for interface stabilization, primarily driven by hydrogen-bond adsorption and hydration effects, which are crucial under high-salinity conditions in industrial processes.

(2) LM-ASQF is maintained within a controllable low-molecular-weight range and displays a unimodal molecular-weight distribution, enabling predictable molecular-weight regulation through adjustment of the initiator dosage. Thermal analysis further indicates that the polymer retains basic structural integrity after thermal exposure below 220 °C, which supports its subsequent evaluation in drilling-fluid systems after high-temperature aging.

(3) In high-salinity, high-temperature-aging, and high-density water-based drilling-fluid systems, LM-ASQF effectively controls fluid loss while maintaining a stable and continuous rheological structure. Its performance is governed primarily by interfacial adsorption and filter-cake densification mechanisms rather than by viscosity enhancement induced by long-chain polymer entanglement. In addition, the LM-ASQF-containing system exhibits low acute biotoxicity under the tested conditions, indicating acceptable environmental compatibility within the scope of the present evaluation. These findings demonstrate the potential of LM-ASQF as a process-compatible fluid-loss additive for complex water-based drilling-fluid applications.

Author Contributions: Conceptualization, G.W. and J.M.; methodology, J.M. and G.W.; validation, J.M., B.H. and G.W.; formal analysis, J.M. and B.H.; investigation, J.M.; resources, B.H. and G.W.; data curation, J.M.; writing—original draft preparation, J.M.; writing—review and editing, G.W. and B.H.; visualization, J.M.; supervision, G.W.; project administration, G.W.; funding acquisition, G.W. All authors have read and agreed to the published version of the manuscript.

Funding: This work was supported by the Sichuan Provincial Regional Innovation Cooperation Project (Grant No. 2024YFHZ0101). The authors gratefully acknowledge the financial support.

Data Availability Statement: The original contributions presented in this study are included in the article. Further inquiries can be directed to the corresponding author.

Conflicts of Interest: Author Bing Huang was employed by the company China National Petroleum Corporation Chuanqing Drilling Engineering Company, Co., Ltd. The remaining authors declare that the research was conducted in the absence of any commercial or financial relationship that could be construed as a potential conflict of interest.

References

1. Fan, W.; Zhuang, G.; Li, Q.; Yuan, P.; Liu, D. Review of Nanoparticles in Water-Based Drilling Fluids: Innovations, Challenges, and Future Directions. *Energy Fuels* **2025**, *39*, 8800–8826. [CrossRef]
2. Zhao, X.; Li, D.; Zhu, H.; Ma, J.; An, Y. Advanced developments in environmentally friendly lubricants for water-based drilling fluid: A review. *RSC Adv.* **2022**, *12*, 22853–22868. [CrossRef] [PubMed]
3. Yang, R.; Jiang, G.; Yang, L.; Li, W.; Deng, T. The effect of inorganic salt on the structure of filter cake of water based drilling fluid. *Socar Proc.* **2014**, 30–38. [CrossRef]
4. Telin, A.; Lenchenkova, L.; Yakubov, R.; Poteshkina, K.; Krisanova, P.; Filatov, A.; Stefantsev, A. Application of hydrogels and hydrocarbon-based gels in oil production processes and well drilling. *Gels* **2023**, *9*, 609. [CrossRef] [PubMed]
5. Min, F.; Du, J.; Zhang, N.; Chen, X.; Lv, H.; Liu, L.; Yu, C. Experimental study on property change of slurry and filter cake of slurry shield under seawater intrusion. *Tunn. Undergr. Space Technol.* **2019**, *88*, 290–299. [CrossRef]
6. Tian, M.; Yang, C.; Huang, Q.; Wang, R.; Su, X.; Xu, P.; Peng, T. Synthesis and Evaluation of High-Temperature-Resistant and Environmentally Friendly Polymer Filter Loss Additives. *Polymers* **2025**, *17*, 792. [CrossRef] [PubMed]
7. Chang, X.; Sun, J.; Xu, Z.; Lv, K.; Dai, Z.; Zhang, F.; Huang, X.; Liu, J. Synthesis of a novel environment-friendly filtration reducer and its application in water-based drilling fluids. *Colloids Surf. A Physicochem. Eng. Asp.* **2019**, *568*, 284–293. [CrossRef]
8. Guo, Y.; Du, M.; Lv, Y.; He, Y.; Jiang, G. Study of three-dimensional reticulated filtration control agent formed by condensation of A-151 in long-lasting, ultra-high-temperature-resistant, salt-resistant, and filtration-loss-reducing. *Chem. Eng. J.* **2024**, *502*, 158047.
9. Liu, L.; Sun, J.; Wang, R.; Qu, Y.; Liu, F.; Yang, J.; Cheng, R.; Gao, S.; Huang, H. Synthesis of a new high temperature and salt resistant zwitterionic filtrate reducer and its application in water-based drilling fluid. *Colloids Surf. A Physicochem. Eng. Asp.* **2022**, *651*, 129730. [CrossRef]
10. Gao, S.; Lin, D.; Li, A.; Deng, L.; Dong, A.; Zhang, J. A zwitterionic polymer filtrate reducer with enhanced anti-polyelectrolyte effect for high-temperature and high-salinity conditions. *Chem. Eng. J.* **2025**, *508*, 161087.
11. Wang, R.; Yang, J.; Liu, L.; Wang, J.; Feng, Z.; Zhang, D.; Gao, S.; Wang, J.; Ren, H.; Hui, B. Investigation on Filtration Control of Zwitterionic Polymer AADN in High Temperature High Pressure Water-Based Drilling Fluids. *Gels* **2022**, *8*, 826. [CrossRef] [PubMed]
12. Li, J.; Sun, J.; Lv, K.; Ji, Y.; Ji, J.; Liu, J. Nano-modified polymer gels as temperature-and salt-resistant fluid-loss additive for water-based drilling fluids. *Gels* **2022**, *8*, 547. [PubMed]
13. Ma, J.; Pang, S.; Zhang, Z.; Xia, B.; An, Y. Experimental study on the polymer/graphene oxide composite as a fluid loss agent for water-based drilling fluids. *ACS Omega* **2021**, *6*, 9750–9763. [PubMed]
14. Bai, X.; Yang, Y.; Xiao, D.; Pu, X.; Wang, X. Synthesis, characterization, and performance evaluation of the AM/AMPS/DMDAAC/SSS quadripolymer as a fluid loss additive for water-based drilling fluid. *J. Appl. Polym. Sci.* **2015**, *132*, 41762.
15. Liu, L.; Pu, X.; Tao, H.; Deng, Q.; Luo, A. Synthesis and characterization of comb-shaped copolymer as a filtration reducer and comparison with counterparts. *RSC Adv.* **2018**, *8*, 11424–11435. [CrossRef] [PubMed]
16. Liu, Y.; Djouonkep, L.D.W.; Yu, B.; Li, C.; Ma, C. Preparation of Ultra-High Temperature Resistant Cyclodextrin-Based Filtration Loss Reducer for Water-Based Drilling Fluids. *Molecules* **2024**, *29*, 2933. [PubMed]
17. Wang, G.; Li, W.; Qiu, S.; Liu, J.; Ou, Z.; Li, X.; Ji, F.; Zhang, L.; Liu, S.; Yang, L.; et al. Application of a core-shell structure nano filtration control additive in salt-resistant clay-free water-based drilling fluid. *Polymers* **2023**, *15*, 4331. [PubMed]
18. Dong, X.; Sun, J.; Huang, X.; Lv, K.; Zhou, Z.; Gao, C. Nano-laponite/polymer composite as filtration reducer on water-based drilling fluid and mechanism study. *R. Soc. Open Sci.* **2022**, *9*, 220385. [PubMed]
19. Yao, X.; Sun, X.; Feng, Q.; Liu, Y.; Liu, Y.; Song, H.; Zhu, K.; Yang, S. Application in oil field drilling with temperature-resistant natural modified filtrate reducer: A review. *Chem. Technol. Fuels Oils* **2023**, *59*, 146–165. [CrossRef]
20. Dong, X.; Sun, J.; Huang, X.; Li, J.; Lv, K.; Zhang, P. Synthesis of a low-molecular-weight filtrate reducer and its mechanism for improving high temperature resistance of water-based drilling fluid gel system. *Gels* **2022**, *8*, 619. [PubMed]
21. Yang, J.; Sun, J.; Wang, R.; Liu, F.; Wang, J.; Qu, Y.; Wang, P.; Huang, H.; Liu, L.; Zhao, Z. Laponite-polymer composite as a rheology modifier and filtration loss reducer for water-based drilling fluids at high temperature. *Colloids Surf. A Physicochem. Eng. Asp.* **2022**, *655*, 130261.

22. Luo, Y.; Lin, L.; Luo, P.; Guo, Y.; Xie, S.; Wang, M.; Xiong, G.; Gu, H. Polymer nanocomposite ADA@ SM as a high-temperature filtrate reducer for water-based drilling fluids and its filtration loss mechanism. *Colloids Surf. A Physicochem. Eng. Asp.* **2023**, *672*, 131701.
23. Lin, Z.; Li, F.; Liu, X.; Su, J. Synthesis of a network-structured polymer with low viscosity effect and its use as filtrate reducer for water-based drilling fluids. *J. Appl. Polym. Sci.* **2023**, *140*, e54581.

Disclaimer/Publisher's Note: The statements, opinions and data contained in all publications are solely those of the individual author(s) and contributor(s) and not of MDPI and/or the editor(s). MDPI and/or the editor(s) disclaim responsibility for any injury to people or property resulting from any ideas, methods, instructions or products referred to in the content.